Relation of coxarthrosis to stresses and morphogenesis

A finite element analysis

Dennis R. Carter[1,2,3], Daniel J. Rapperport[3], David P. Fyhrie[1,3] and David J. Schurman[2]

We calculated subchondral deformations and stresses in the femoral head and acetabulum during weight bearing using finite element models. Areas of high joint contact pressures on the femoral head were shown to correspond to high hydrostatic compression in subchondral bone. The magnitude of the subchondral bone compressive hydrostatic stress correlated with cartilage thickness and was highest in the superior femoral head and moderate at the acetabular roof. The seldom contacting surfaces of the medial-inferior and peripheral areas of the femoral head and the roof of the acetabulum had lower hydrostatic compression and significant subchondral bone tensile strains tangential to the joint surface. Initial cartilage fibrillation and osteophyte formation are often found in these areas. These findings suggest that fluctuating hydrostatic pressure inhibits vascular invasion and the degeneration and ossification of articular cartilage. The generation of tensile strain may promote the degenerative process by direct mechanical mechanisms. Additionally, since tensile strains are associated with a reduction in the compressive hydrostatic stresses in the cartilage and an increase in shear stresses, their presence may permit or promote vascular invasion, cartilage degeneration, and osteophyte formation. These mechanical principles in arthrosis are the same as those that have been previously demonstrated to guide the degeneration and ossification of the cartilage primordium during skeletal morphogenesis. In this sense, arthrosis may be viewed as the final stage in the degeneration and ossification of the cartilage anlage.

It is generally accepted today that arthrosis begins as a degeneration of the cartilage (Kempson et al. 1971), and bone remodeling and osteophyte formation are viewed as secondary events (Danielsson 1964, Ahlbäck 1968). Radin et al. (1973) proposed that subchondral bone sclerosis was the primary event and that subsequent cartilage damage was a mechanical result of the stiffness changes in the remodeled subchondral bone.

We report finite element analyses of the hip used to simulate typical loading conditions. The results are compared with the regional histologic and morphologic degenerative changes observed by others. Our objective was to establish the role that the cyclically applied stresses play in the degenerative process.

Departments of [1]Mechanical Engineering and [2]Surgery, Stanford University, Stanford, California, and the [3]Veterans Administration Medical Center, Rehabilitation R&D Center, Palo Alto, California, U.S.A.

Materials and methods

Two finite element computer models were employed to calculate stress distributions in the femoral head and acetabulum. The results of these models were then compared with the previous observations of joint pathology. The first model was a two-dimensional, nonlinear contact model of the femoral head and acetabulum. We relied on this model primarily to provide information on the acetabular side of the joint.

2-D joint contact model

A two-dimensional model was generated from a roentgenogram of a 4-mm slice cut normal to the acetabulum and going through the pubis. The basic geometry, material properties, and boundary conditions used for this model have been reported by Rapperport et al. (1986). The femoral head was modeled as having a circular surface, which was mated with a congruent circular acetabular socket. The surface discontinuity at the foveal notch was not included in the model; however, the low modulus of the surrounding rarefied bone was incorporated. Although there is some question about the geometries of the femoral head and the acetabulum (Bullough et al. 1973, Clarke & Amstutz 1975, Rushfeldt et al. 1981), our models assumed congruency of the mating surfaces and sphericity of the femoral head and corresponding acetabular socket as a first approximation.

The plane strain finite element model consisted of 1,120 nodes comprising 1,271 quadrilateral and triangular elements and 30 contact elements. For the model boundary conditions, the pubic symphysis was allowed to displace in the sagittal plane and was free to rotate. The sacroiliac joint was free to displace only in the plane of the joint and the extreme margin of cortical bone in the ilium was rigidly fixed. Four-noded frictionless contact elements were incorporated at the joint surface so that intraarticular contact pressures could be calculated as the proximal femur was pushed into the socket.

To account for the varying material properties, the model was partitioned into 24 regions of different elastic constants. Material isotropy was assumed in each region. Crude representations of articular cartilage (one element thick) were included on both the femoral and acetabular surfaces, but calculated cartilage stresses are not reported here because of their inherent inaccuracies. This study reports the results obtained as a region of subchondral bone successively stiffened in the model (Figure 1). In the normal hip model the region was assumed to have an elastic modulus of 700 MPa. The influence of increasing this modulus to 1,400 and 5,000 MPa was determined.

The resultant femoral load angles in the analyses shown here were 20° medial of vertical. A load magnitude of 1,000 N/cm was chosen so that maximum bone stresses were approximately 30 per cent of ultimate strength, as determined by Carter & Hayes (1976).

3-D femoral head model

The geometry for this idealized model was adapted from measurements taken from the excised femur of a normal 55-year-old white male. The finite element model was axisymmetric about the femoral neck axis, so only half of the head and neck were represented (Figure 2). The head was

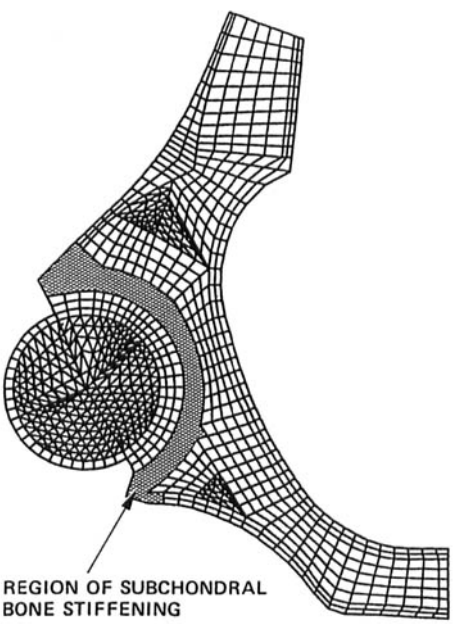

Figure 1

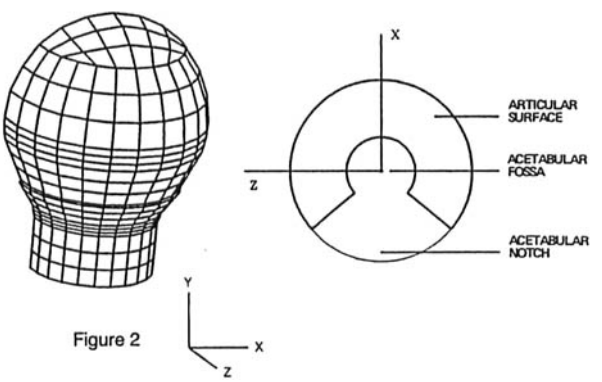

Figure 2

Figure 1. The element mesh with an indication of the region of subchondral bone stiffening used in the 2-D contact model.

Figure 2. The finite element mesh of the proximal femur model and the idealized acetabular contact area that was assumed in the analysis.

50.8 mm in diameter and the head and neck together stood 76-mm high. The neck was 30.4-mm in diameter and had a cortical shell 1.0-mm thick with one element through the thickness. The interior of the neck was completely filled with cancellous bone, as was the head.

The material properties used were symmetric about the axis of the head and neck and were not particularly complex. The cortical values (Modulus E = 5,000 MPa, Poisson's ratio ν = 0.32) were taken from Murray et al. (1984), and the cancellous bone values were chosen to be consistent with the range of cancellous bone moduli reported by Brown & Ferguson (1980). The femoral head cancellous bone was assigned a modulus of 1,000 GPa. The femoral neck cancellous bone was assigned modulus values of 500 GPa near the cortical shell and 400 GPa in the interior. All the cancellous bone was assigned a Poisson's ratio of 0.2. Neither articular cartilage nor a specific layer representing a subchondral bone plate was represented in the model. Simkin et al. (1980) showed that the subchondral plate in all convex joints is very thin compared with that in concave joints. In the femoral head, a mean subchondral thickness of 0.4 mm was measured as compared with 2.6 mm on the acetabular side. It is difficult to represent such a thin layer in a finite element model and the low stiffness role of that layer (Brown & Vrahas 1984) will have little influence on the qualitative results reported here.

The model consisted of 1,453 trilinear (8-node) brick elements and was fixed along the lower periphery of the cortical bone of the neck (Fyhrie 1986). Nodes on the symmetry plane were constrained to move in that plane only.

The loading on the natural hip is transmitted through the lunate cartilage of the acetabulum. For our analyses, we generated an idealized acetabular surface, i.e., a 25.4-mm-radius hemisphere with a 15.9-mm-wide articular surface and a 100-degree-wide acetabular notch centered on the acetabular fossa (Figure 2). We assumed that the pressure distribution on the idealized lunate cartilage is zero on its edges and follows the square root of the sine both across the surface and around its length. This causes the maximum pressure to be at the midline of the cartilage on the vertical axis in Figure 2.

The pressure was converted into consistent nodal loads for application to the model (Figure 3). The large arrow in Figure 3 is the resultant load direction of the entire load (we only see half of the symmetric loading in this figure). The resultant load lies in the X-Y plane at an angle of 43.3 degrees to the Y-axis (which lies along the femoral neck axis) and passes through the geometric center of the femoral head. The resultant load magnitude applied was 2,421 N, approximately three to four times the body weight and therefore well within the physiologic range. The maximum contact pressure at the superior head was 5 MPa. Though idealized, the joint contact pressures used are qualitatively and quantitatively consistent with experimentally determined pressure distributions (Brown & Shaw 1983, Day et al. 1975, Rushfeldt et al. 1981).

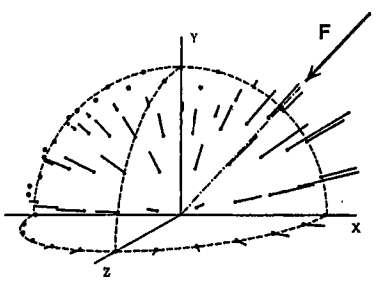

Figure 3

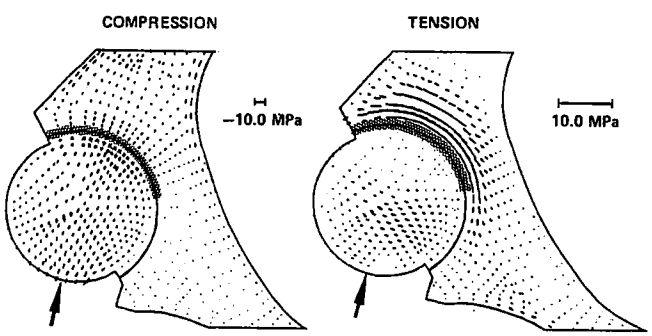

Figure 4

Figure 3. The orientation of the load resultant (F = 2421N) on the femoral head and the distribution of nodal forces at the contact surface. The length of the surface lines corresponds to contact pressure magnitudes (maximum 5 MPa). Unloaded nodes are indicated by small circles.

Figure 4. The distribution of principal stresses in the 2-D contact model. The shaded area is where contact occurs.

Results

Stresses and strains in the subchondral bone

The 2-D contact model analysis predicted stress fields in the femoral head (Figure 4) that were qualitatively consistent with the 3-D predictions. The highest stresses were under the area of maximum contact pressure where a state of biaxial compression was calculated in the femoral head. This finding agreed with the prediction of high-magnitude, compressive, hydrostatic stresses near the contact surface of the 3-model.

The state of stress on the acetabular side of the joint, however, differed distinctly from the femoral side in the region of high-contact stresses (Figure 4). Due to the concavity of the acetabulum, the femoral head tended to push into the acetabulum to create tangentially oriented tensile strains and stresses in the subchondral area. The subchondral bone at the roof of the acetabulum was exposed to biaxial compression-tension stresses. In a single-phase continuum material, hydrostatic stress could be thought of as the local hydrostatic pressure within a material. The hydrostatic stress in a plane strain model was calculated as $P = (1 + \nu)\ \sigma_1 + \sigma_2)/3$, where σ_1 and σ_2 are the principal stress. The hydrostatic stresses on the femoral side were approximately equal to the contact pressure. At the region of high-contact pressure, the surface pressure was about 4 MPa and the subchondral hydrostatic stress on the femoral side about 3.5 MPa. On the corresponding acetabular side, however, the hydrostatic stresses were everywhere *less than half* of the contact pressure. The lower hydrostatic stresses are a direct reflection of the tensile stresses and strains in the subchondral bone on this concave surface. The acetabular hydrostatic compressive stresses were highest at the roof, because that was the surface of highest contact pressures. The acetabular cartilage was thickest at the roof, but was always thinner than that on the mating surface of the femoral head (Kurrat & Oblerlander 1979), which, according to our analyses, experienced greater compressive hydrostatic stresses at locations equidistant from the joint surface.

The effect of subchondral stiffening (sclerosis) on the contact pressure distribution and maximum principal strains in the acetabular subchondral bone is shown in Figure 5. The articular surface contact pressure was nearly identical to the subchondral bone principal stress component acting in a direction normal to the joint surface. Because the elastic modulus of the subchondral bone was from 700 to 1,400 to 5,000 MPs, there was a negligible change in the joint contact pressure magnitude and distribution. However, the maximum principal strains in the acetabular subchondral bone are significantly reduced, since their magnitude was roughly inversely proportional to the bone modulus. The largest value of maximum principal strain decreased from approximately 0.4

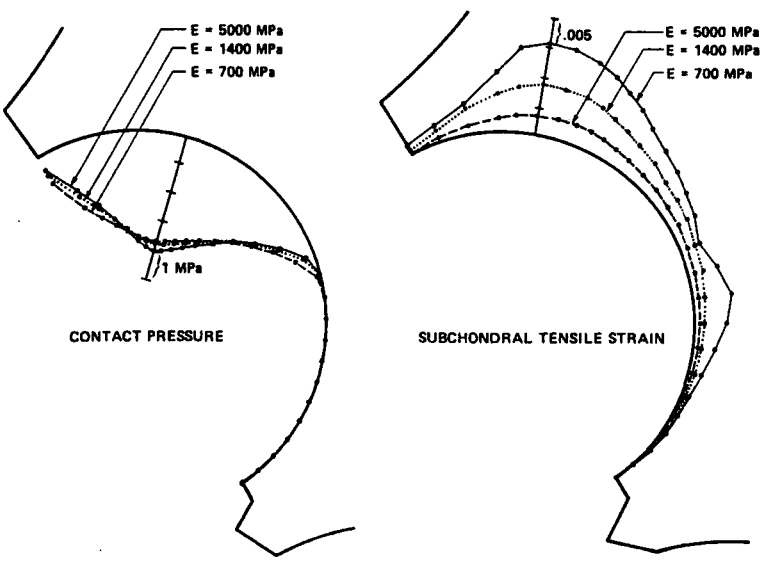

Figure 5. The distributions of surface contact pressure and acetabular subchondral tensile strains calculated for different values of subchondral bone modulus (E).

to 0.07 per cent. In the 3-D femoral-head model, subchondral bone tensile strains (Figure 6) were also reduced when the modulus of the cancellous bone was increased.

The contact pressures on the 3-D femoral-head model were assumed to be distributed around the lunate cartilage, so that the highest pressures (maximum 5.0 MPa) were at the superior surface. This loading condition tended to squeeze the head in such a manner as to create substantial hydrostatic compressive stresses and strains directly under the loaded area. The surface areas that were not loaded tended to bulge outward under load, resulting in tangentially oriented tensile stresses and strains. The resulting distributions of subchondral hydrostatic stresses and maximum strains reflected this pattern of deformation (Figure 6). The hydrostatic stress, P, is the average principal stress; $P = (\sigma_1 + \sigma_2 + \sigma_3)/3$. In our femoral head model, the areas of compressive hydrostatic stresses at the surface directly under the load correlated quite well both in location and magnitude with the applied surface pressure. These areas also correlate with the areas of thick cartilage (Kurrat & Oblerlander 1979), which are not generally initial sites of degenerative change. The noncontact surface areas with high tangential tensile strains and low compressive hydrostatic stress, on the other hand, are the sites where the cartilage is thin and initial degeneration and osteophyte formation occur.

Interior of the femoral head

The contact pressures at the joint surface tended to squeeze the head and create high compressive hydrostatic stresses in the subchondral bone under the contact area. The region of compressive hydrostatic stresses was not confined to the superficial areas, but extended into the femoral-head cancellous bone. Both the 2-D and 3-D models indicated the region of highest compressive hydrostatic stress to be a conical region under the area of maximum surface pressure. These stresses are directly proportional to the dilatational or volumetric strain (volume change/initial volume) experienced by the trabecular bone regions in the femoral head. Contours of constant volumetric strain in the interior regions of the head are displayed in Figure 7 for a central coronal slice through the 3-D model. The conical region dilatational strains showed a strong correlation with the region of bone, vascularity, marrow, and cystic changes in the later stages of arthrosis previously reported by others.

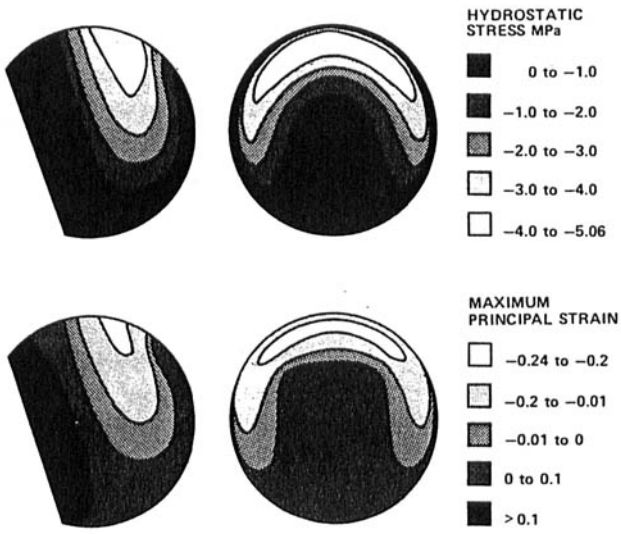

Figure 6

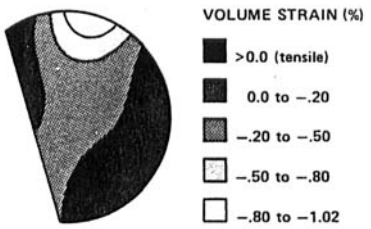

Figure 7

Figure 6. Contour maps showing the distributions of hydrostatic stress and maximum principal strain on the subchondral surface of the 3-D femoral head finite element model.

Figure 7. Distribution of volume (dilatational) strain in the interior, central coronal section of the 3-D femoral head model.

Discussion

In this study, we have used static analyses to simulated the cyclically applied loading of the hip joint at one moment in time with the limb in one specific orientation. The loads on the hip and the orientations of the limbs are, in fact, complicated, time-varying functions. The actual stress-and strain field will vary in magnitude and locations as full range of motion is achieved during various activities. The regions of hydrostatic stress and maximum strain will thus sweep throughout the subchondral bone and over the joint surface. We would expect that the entire articular surface will contact the lunate cartilage and local compressive hydrostatic stresses will be created at some point in time. The role of stresses in regulating joint biology and disease must be established by the cumulative influence of these load excursions. The loading condition used in our study was chosen because we felt that it would tend to have a major influence on the joint pathology, for it or similar loadings are so often applied during daily activities. It serves us as a preliminary indicator of major trends in the stress patterns.

The initial degenerative area in the acetabulum is located where the mating surface cartilage of the femoral head is the thickest and rarely the site of initial degeneration. To explain this apparent anomaly, Bullough et al. (1973) cite the work of Greenwald & O'Connor (1971) and Greenwald & Haynes (1972) and suggest that hip-joint incongruities in young individuals exist such that the acetabular roof does not contact the femoral head under load magnitudes of 20 to 50 per cent body weight. Because joint congruity increases with age, full contact at the dome will be achieved at relatively low loads in older individuals (Greenwald & Haynes 1972). Following the arguments of Harrison et al. (1953) regarding the femoral head, Bullough et al. (1973) contend that sites of initial degeneration in both the acetabulum and femoral head are a result of habitual noncontact (Figure 8). Some other researchers have been reluctant to accept this hypothesis because during normal walking the hip forces are approximately three times the body weight, resulting in the high-contact pressures at the roof of the acetabulum recorded with an instrumented hemiprosthesis in vivo (Hodge et al. 1985) and with normal hip joints in vitro (Brown & Shaw 1983, Day et al. 1975).

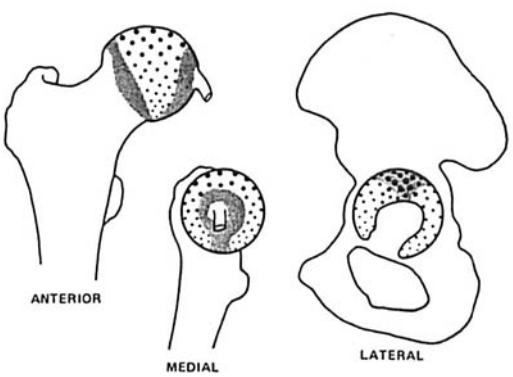

Figure 8. The areas of initial degeneration (shaded) are shown in relation to the areas of surface contact (stippled). The more heavily stippled areas indicate greater contact pressure.

An important concept that emerges from our study is that joint contact pressures are not the same as the tissue pressures, but are more closely related to the hydrostatic stresses. In a one-phase material, the hydrostatic stresses are the tissue pressures. In a complex material like trabecular bone, the continuum-model hydrostatic stresses result in complicated stress distributions in the trabeculae and volume change and/or hydrostatic pressure in the nonmineralized tissue components.

Within convex joint surfaces such as the femoral head, the contact pressures normal to the joint surface will create in subchondral bone principal compressive stresses in directions tangential to the joint surface. This is a characteristic of all arched or domed structures. Because the hydrostatic stress is the average of the three principal stresses, the hydrostatic stresses will be compressive and comparable in magnitude to the applied surface pressure in a convex joint. In a pure state of hydrostatic compression, no tensile strains will be created. When the same surface pressure is applied to concave joint surfaces, such as the acetabulum, a very short distance from the surface (in the subchondral bone), the principal stresses tangential to the surface will be tensile, as will the maximum principal strain. The hydrostatic stresses will therefore not be as compressive as on the convex side. It is thus apparent that, although the contact pressures are the same on both sides of the joint, the hydrostatic stresses at locations equidistant from the surface are very different. This

difference is manifested morphologically by the more extensive ossification of the cartilage in the concave surface during joint morphogenesis, resulting in a thinner cartilage layer.

Articular cartilage is avascular and consequently has a low oxygen tension and metabolic rate compared with bone and other vascular tissues (Stockwell 1983). One would expect that it would be more difficult to develop and maintain a vascular system in the regions of high-magnitude, intermittent, compressive hydrostatic stress to which articular cartilage is exposed (Kuettner & Pauli 1983). Because vascularity is necessary to maintain bone, it is reasonable that the thickest articular cartilage is found in areas of highest compressive hydrostatic stresses. Conversely, one might expect low-magnitude compressive stress to be associated with thin cartilage because cartilage calcification with its associated increased vascularity is not as inhibited. This theory can be applied to other convex-concave joints in the body in addition to the hip joint. Convex joint surfaces have their greatest cartilage thickness at the region of highest contact pressure. On the mating location on the concave surface, however, the cartilage is always thinner (Warwick & Williams 1973).

In the development of the chondro-osseous epiphysis, the bone is created by the progressive expansion of the secondary ossific nucleus. As the front of ossification proceeds towards the articular surface, the layer of articular cartilage at the bone end begins to be defined. We believe that the ossification front slows as it approaches areas of intermittent hydrostatic pressure. The distribution of cartilage thickness is, therefore, a reflection of the stress state near the joint surface. Directly at the surface, cartilage will exist (either on a convex or a concave surface) and will be exposed to intermittent hydrostatic pressure. The thickness of the cartilage in a specific area, however, is related to the magnitude and frequency of intermittent hydrostatic pressure at distances from the surface.

Whereas compressive hydrostatic stresses appear to protect cartilage viability, the generation of tensile strains in the subchondral bone may promote the degenerative process. The areas of initial degenerative change on both the femoral and the acetabular sides correspond to the areas of subchondral bone tensile strains. Because our models did not include a specific structure to represent the subchondral plate, the strains that we calculated are probably somewhat high for the area of calcified cartilage. The subchondral plate would tend to resist deformation and protect the cartilage from excessive tensile strains. However, since there is strain continuity from the subchondral bone to the cartilage, there will always be a tendency to create tensile strains in the deep zones of the calcified cartilage. Although the magnitudes may be reduced, the distributions of these strains will be nearly identical to those shown in this study. The effect of such strains on the local remodeling processes is unknown. However, many have postulated that the creation of tensile strains in cartilage may promote mechanical damage and contribute to degeneration (Askew & Mow 1978, Freeman 1975, Kempson et al. 1971, Weightman 1976).

The distribution of compressive volumetric strains within the femoral-head cancellous-bone bed probably influences the pathology observed in late stages of arthrosis. The region directly beneath the area of high joint contact pressures is often delineated by an inverted conical zone wherein the marrow, bone trabeculae, and vascular pattern have distinctive features. The marrow is unlike hemopoietic or fatty marrow, and is described by Harrison et al. (1953) as being fibrous with intercellular fluid suggestive of local edema. The bone trabeculae are thickened and sometimes consist of healthy lamellae covering dead bone, appearing as a sclerotic region roentgenographically. There is arterial hyperemia and the vascular pattern is dominated by a state of venous engorgement. The fibrous tissue that comprises the cysts may be loose and myxoid, dense, or fibrocartilaginous. There is a paucity of blood vessels in this fibrous tissue. The cystic areas are surrounded by dilated vessels of a sinusoidal pattern.

When compressive volumetric strains are created in an area of cancellous bone, the volume of marrow, fluid, and bone in that region must be reduced. Because fluid flow is easily influenced by small pressure gradients, the volume reduction will be achieved primarily by a reduction in the local volume of the vascular bed. The bone supports the stresses, but the volume loss is primarily in the vasculature and may be associated with impaired perfusion. In advanced disease,

high-stress magnitudes in the cancellous bone cause progressive fracture and collapse of trabeculae. This collapse will further increase the compressive volumetric strains and constrict the vascular bed. Local edema due to tissue injury could cause an increase in the tissue pressure and further impair vascular perfusion. The fibrous tissue that constitutes bone cysts in this region may never be converted to bone because vascular insufficiency promoted by intermittent compressive hydrostatic stresses and tissue swelling effectively inhibit the formation of a vascular supply needed to produce and maintain bone.

The observations concerning relationships between stress fields and joint morphology and pathology for the hip can also be extended generally to other joints. Simkin et al. (1980) found that concave joints, such as the glenohumeral and acetabulum, tend to have very thick subchondral bone plates compared with convex joints, such as the humerus and femoral head. They hypothesized that this difference is due to the difference in stress transmission in the subchondral regions. They further conjectured that differences in stress fields may explain why idiopathic osteonecrosis and osteochondritis dissecans occur only on the convex side of the joint. Solomon (1985) reviewed mechanisms of idiopathic osteonecrosis. Bone death in such cases is always due to ischemia or a disparity between the oxygen need of the bone cell and the ability of the local circulation to supply that need. The results of our study point unmistakably to the conclusion that compressive hydrostatic stresses and the associated volumetric strains contribute to the vascular insufficiency on the convex side of the joint.

Our hypothesis is that idopathic degenerative joint disease is, in fact, the final stage of the ossification of the cartilage anlage. The degeneration and ossification of the anlage is promoted by cyclic shear stresses and inhibited by cyclic hydrostatic stresses (Carter et al. in press). Intermittent shear stresses result in the dissipation of mechanical energy in the cartilage. The transduction of this mechanical energy to biochemical processes may accelerate the normal sequence of cartilage proliferation, maturation, degeneration, and ossification. Increases in load magnitudes caused by increased physical activities, obesity, ligament injury, or fracture will increase the stresses in cartilage and affect the time of onset and severity of arthrosis. Genetically related sensitivity to loading history may also be associated with the severity of the degenerative process.

References

Ahlbäck S. Osteoarthritis of the knee. A radiographic study. Acta Radiol (Diagn) (Stockh) 1968;(Suppl 277):7–72.

Askew M J, Mow V C. The biomechanical function of the collagen fibril ultrastructure of articular cartilage. J Biomech Eng 1978;100:105–15.

Brown T D, Ferguson A B Jr. Mechanical property distributions in the cancellous bone of the human proximal femur. Acta Orthop Scand 1980;51:429–37.

Brown T D, Shaw D T. In vitro contact stress distributions in the natural human hip. J Biomech 1983;16(6):373–84.

Brown T D, Vrahas M S. The apparent elastic modulus of the juxtarticular subchondral bone of the femoral head. J Orthop Res 1984;2(1):32–8.

Bullough P, Goodfellow J, O Conner J. The relationship between degenerative changes and load bearing in the human hip. J Bone Joint Surg (Br) 1973;55(4):746–58.

Carter D R, Fyhrie D P, Whalen R T. Trabecular bone density and loading history: regulation of connective tissue biology by mechanical energy. J Biomechanics (in press).

Carter D R, Fyhrie D P, Whalen R T, Orr T E, Schurman D J, Rapperport D J. Control of chondro-osseous biology by mechanical energy. In: Biomechanics: Principles and applications (Selected proceedings of the Fifth Meeting of the European Society of Biomechanics).(Eds. Bergmann G, Kolbel R & Rohlmann, A) (in press).

Carter D R, Hayes W C. Bone compressive strength: the influence of density and strain rate. Science 1976;194(4270):1174–6.

Carter D R, Orr T E, Fyhrie D P, Schurman D J. Influences of mechanical stress on prenatal and postnatal skeletal development. Clin Orthop 1987; 219:237–250.

Carter D R, Wong M. Mechanical stresses and endochondral ossification in the chondroepiphysis. J Orthop Res (in press).

Clarke I C, Amstutz H C. Human hip joint geometry and hemiarthroplasty selection. In: The Hip, Proceedings of the Third Open Scientific Meeting of the Hip Society, C.V. Mosby Co, St Louis 1975:63–5.

Danielsson L G. Incidence and prognosis of coxarthrosis. Acta Orthop Scand 1964;(Suppl 66).

Day W H, Swanson S A, Freeman M A. Contact pressures in the loaded human cadaver hip. J Bone Joint Surg (Br) 1975;57(3):302–13.

Freeman M A. The fatigue of cartilage in the pathogenesis of osteoarthrosis. Acta Orthop Scand 1975;46(3):323–8.

Fyhrie D P. Stress analysis and design of proximal femoral prostheses. Ph. D. Dissertation, Stanford University 1986.

Greenwald A S, O'Connor J J. The transmission of load through the human hip joint. J Biomechanics 1971;4:507–28.

Greenwald A S, Haynes D W. Weight bearing areas in the human hip joint. J Bone Joint Surg (Br) 1972;54(1):157–63.

Harrison M H M, Schajowitz F, Trueta J. Osteoarthritis of the hip: A study of the nature and evolution of the disease. J Bone Joint Surg (Br) 1953;35:598–626.

Hodge W A, Fijan R, Mann R W, Harris W H. Preliminary in vivo pressure measurements in a human acetabulum. Trans. 31st Annual ORS 1985;10:284.

Kempson G E, Spivey C J, Swanson S A, Freeman M A. Patterns of cartilage stiffness on normal and degenerate human femoral heads. J Biomech 1971;4(6):597–609.

Kuettner K E, Pauli B V. Vascularity of cartilage. In: Cartilage: Structure, Function and Biochemistry (Ed. Hall, B K). Academic Press, New York 1983;3:281–312.

Kurrat H J, Oberlander W. The thickness of the cartilage in the hip joint. J Anat 1978:126(1):145–55.

Murray R P, Hayes W C, Edwards W T, Harry J D. Mechanical properties of the subchondral plate and the metaphyseal shell. Trans 30th Annual ORS 1984;9:197.

Radin E L, Parker H G, Pugh J W, Steinberg R S, Paul I L, Rose R M. Response of joints to impact loading. 3. Relationship between trabecular microfractures and cartilage degeneration. J Biomech 1973;6(1): 51–7.

Rapperport D J, Carter D R, Schurman D J. Contact finite element stress analysis of the hip joint. J Orthop Res 1985;3(4):435–46.

Rushfeldt P D, Mann R W, Harris W H. Improved techniques for measuring in vitro the geometry and pressure distribution in the human acetabulum I. Ultrasonic measurement of acetabular surfaces, sphericity and cartilage thickness. J Biomech 1981;14(4):253–60.

Rushfeldt P D, Mann R W, Harris W H. Improved techniques for measuring in vitro the geometry and pressure distribution in the human acetabulum II. Instrumented endoprosthesis measurement of articular surface pressure distribution. J Biomech 1981;14(5):315–23.

Simkin P A, Graney D O, Fiechtner J J. Roman arches, human joints, and disease: differences between convex and concave sides of joints. Arthritis Rheum 1980;23(11):1308–11.

Solomon L. Mechanics of idiopathic osteonecrosis. Orthop Clin North Am 1985;16:655.

Stockwell R A. Metabolism of cartilage. In: Cartilage: Structure, Function and Biochemistry (Ed. Hall, B K). Academic Press, New York 1983;3:253–80.

Warwick R, Williams P L. Grays Anatomy. W.B. Saunders Co., Philadelphia 1973.

Weightman B. Tensile fatigue of human articular cartilage. J Biomech 1976;9(4):193–200.

Acknowledgements

The work was supported by the Veterans Administration Rehabilitation R&D funding and by NIH grants AM 32378 and AM 01163 (RCDA for Dr. Carter).